J Biol Inorg Chem (2013) 18:95–101
DOI 10.1007/s00775-012-0954-4

ORIGINAL PAPER

Fe–O versus O–O bond cleavage in reactive iron peroxide intermediates of superoxide reductase

Amr Ali Ahmed Ali Attia · Daniela Cioloboc · Alexandru Lupan · Radu Silaghi-Dumitrescu

Received: 26 February 2012 / Accepted: 15 October 2012 / Published online: 8 November 2012

Abstract It is generally accepted that the catalytic cycles of superoxide reductases (SORs) and cytochromes P450 involve a ferric hydroperoxo intermediate at a mononuclear iron center with a coordination sphere consisting of four equatorial nitrogen ligands and one axial cysteine thiolate *trans* to the hydroperoxide. However, although SORs and P450s have similar intermediates, SORs selectively cleave the Fe–O bond and liberate peroxide, whereas P450s cleave the O–O bond to yield a high-valent iron center. This difference has attracted the interest of researchers, and is further explored here. Meta hybrid DFT (M06-2X) results for the reactivity of the putative peroxo/hydroperoxo reaction intermediates in the catalytic cycle of SORs were found to indicate a high-spin preference in all cases. An exploration of the energy profiles for Fe–O and O–O bond cleavage in all spin states in both ferric and ferrous models revealed that Fe–O bond cleavage always occurs more easily than O–O bond cleavage. While O–O bond cleavage appears to be thermodynamically and kinetically unfeasible in ferric hydrogen peroxide complexes, it could occur as a minor (significantly disfavored) side reaction in the interaction of ferrous SOR with hydrogen peroxide.

Keywords Superoxide reductase (SOR) · Ferric peroxo · Superoxide · Hydrogen peroxide · Non-heme iron

Introduction

Superoxide reductases (SORs) catalyze the reduction of superoxide to hydrogen peroxide. They are categorized into one-iron SORs (containing a catalytic site with non-heme iron [1–4]) and two-iron SOR (containing, in addition to a catalytic site similar to that of 1Fe-SORs, a rubredoxin-like $[Fe^{3+}(SCys)_4]$ center) [3, 5, 6]. The ligands of the ferric resting state are a carboxylate oxygen *trans* to a cysteinate together with four equatorial histidines, which comprise a pseudo-octahedral conformation [7, 8].

As depicted in Fig. 1, the generally accepted catalytic cycle of SORs is initiated by the binding of the superoxide to the ferrous site to produce a formally ferrous superoxo/ferric peroxo state. A subsequent protonation step leads to a ferric hydroperoxo complex; a second protonation leads to the formation of hydrogen peroxide, which is liberated from the active site coordinated with a carboxylate in its resting ferric form. A one-electron reduction step then leads back to the starting ferrous state. In addition, particularly for SORs from *Archaeoglobus fulgidus* and *Desulfoarculus baarsii*, a pathway has also been proposed in which the ferric center binds a solvent molecule after the liberation of hydrogen peroxide and prior to the resting ferric state [9–12].

The identities of the reactive intermediates are yet to be confirmed. Pulse radiolysis as well as resonance Raman and Mössbauer spectroscopic methods were used in several studies to identify the reactive intermediates in different SOR classes. Among others, Emerson et al. [12] reported pulse radiolysis data on the recombinant two-iron SOR

Electronic supplementary material The online version of this article (doi:10.1007/s00775-012-0954-4) contains supplementary material, which is available to authorized users.

A. A. A. A. Attia · D. Cioloboc · A. Lupan · R. Silaghi-Dumitrescu (✉)
Department of Chemistry and Chemical Engineering, "Babes-Bolyai" University, 1 Mihail Kogălniceanu str, 400084 Cluj-Napoca, Romania
e-mail: radu.silaghidumitrescu@gmail.com; rsilaghi@chem.ubbcluj.ro

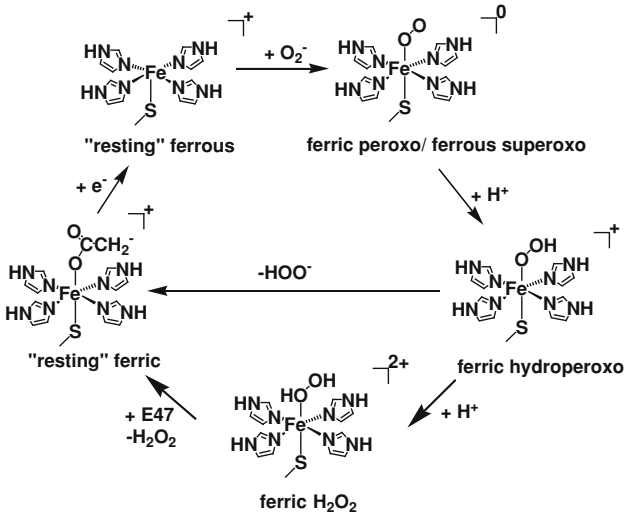

Fig. 1 Catalytic cycle proposed for superoxide reductases; two alternative pathways are possible from the ferric hydroperoxo state—one directly proton dependent and one indirectly or not proton dependent (involving unilateral dissociation of the hydroperoxide from the iron)

from *Desulfovibrio vulgaris* and observed an intermediate that absorbed at approximately 600 nm, which was described as a ferric (hydro)peroxo species that disappeared with the formation of the resting ferric active site. These results were further supported by Huang et al. [13], who performed a stopped-flow mixing study on the same enzyme. Mathé et al. [14, 15] carried out a study on the active site of SORs from *D. baarsii* and *Treponema pallidum* and showed, by means of resonance Raman spectroscopy, a high-spin Fe^{3+} peroxo species as a reactive intermediate—results that were supported by Horner et al. [16] using Mössbauer spectroscopy. A ferric peroxo intermediate was also supported by Rodrigues et al. [10] based on a study involving pulse radiolysis and stopped-flow kinetics on an SOR from *A. fulgidus*. On the other hand, using the same spectroscopic methods, Testa et al. [17] showed that an SOR from *Giardia intestinalis* reacts with superoxide to form a ferric (hydro)peroxo bound active center, which rapidly decays into a glutamate-bound resting ferric state with no evidence for the formation of a solvent-bound active center.

Furthermore, in studies on an SOR from *D. baarsii*, reported by Bonnot et al. [11], the authors obtained experimental and theoretical evidence through pulse radiolysis and TD-DFT calculations that the first reactive intermediate is a ferrous superoxo adduct, and proposed a catalytic mechanism in which ferrous superoxo and ferric hydroperoxide are key intermediates. In addition, the authors provided evidence that the absorption spectrum recorded at 625 nm in previous works was in fact attributable to photochemical processes that took place during the transient step in the catalytic cycle, and proved that this spectrum disappears when the photochemical processes are absent [18].

Katona et al. [19] were able to successfully trap the ferric-(hydro)peroxo species in crystals of SOR, and reported (based on X-ray diffraction data and Raman spectra recorded in crystals) a ferric hydro(peroxo) intermediate in which the hydro(peroxo) adduct is bound in an end-on conformation.

We previously reported an initial density functional study where geometric and electronic structures of various possible SOR reaction intermediates were described, including unprotonated as well as mono- and diprotonated ferric peroxo adducts. Based on thermodynamic considerations, we concluded that the experimentally observed 600 nm intermediate is most likely ferric hydroperoxo. ZINDO/S-CI electronic absorption spectrum simulations revealed that the absorption maximum at 600 nm in such a complex would arise from ligand to metal charge transfer: mainly thiolate → iron, with a minor peroxide → iron contribution. Low-spin states ($S = 1/2$) were predicted for the peroxo/hydroperoxo intermediates. It was pointed out that the design of the SOR site, especially its solvent exposure, which allows unrestricted access of protons to both oxygen atoms of the iron-bound peroxide, is crucial to achieving hydrogen peroxide formation and liberation at the expense of the oxygen–oxygen bond cleavage observed in related ferric peroxo intermediates seen in oxidases such as cytochrome P450 [20]. On the other hand, TD-DFT calculations by Bonnot et al. [11] revealed a broad absorption band at 614 nm which corresponded to a similar spectrum recorded by pulse radiolysis for a ferrous superoxo species; such a species is therefore considered by the authors to be the first reaction intermediate in the catalytic cycle of SOR.

X-ray diffraction models of different SOR monomers obtained by Katona et al. [19] were reported and showed a peroxide adduct with an orientation that induces the thiolate iron peroxide atoms to adapt a non-coplanar conformation resulting in a nonoptimal π-orbital overlap that weakens the bond between iron and oxygen.

The SOR axial thiolate was computed to have an apparently modest *trans* effect on peroxo and hydroperoxo ligands; however, its *trans* effect on nitric oxide was found to be substantial, in line with prior experimental observations [21, 22]. Furthermore, the thermodynamic effect of the thiolate was found to be crucial to favoring protonation of the iron-bound peroxide (note that alternative anionic ligands were computed to perform just as well as thiolate) [22].

Another study was reported by Dey and Solomon in which the fate of Fe–O cleavage of the ferric (hydro)peroxo intermediate of SORs was investigated by DFT for

both high- and low-spin states and for *cis* and *trans* orientations of the thiolate ligand with respect to the (hydro)peroxo ligand. A *trans* thiolate effect was noted (in the form of Fe–O bond elongation and a reduction in the Fe–O vibrational frequency) regardless of the spin state and the orientation of the *trans* thiolate ligand when compared to *trans* ammine models [23], which is somewhat in line with our own results obtained when examining the effects of *cis* and *trans* anionic ligands on ferric hydroperoxo moieties, including SOR models [22, 24]. Such results are in accord with the promotion of hydrogen peroxide liberation over O–O cleavage [23]. In agreement with our previous predictions [20], Dey et al. [23] found a low-spin ground state for the SOR ferric hydroperoxo intermediate. They also found that cleavage of the O–O bond in an SOR ferric-hydroperoxo intermediate would require ~20–30 kcal/mol (depending on the spin state); Fe–O bond cleavage was computed to entail relatively low energies, but would not lead to well-defined minima, as the computations were performed on small models in vacuum [23].

Solomon and co-workers further examined the resting high-spin ferric site of SORs by ligand K-edge XAS and computational methods, providing detailed information on the Fe–S bond covalency and its relevance to the catalytic cycle, and affording unprecedentedly detailed information on the electronic factors controlling superoxide reduction in SOR. Importantly, their DFT results favored a high-spin state for the putative hydroperoxo reaction intermediate [25].

Further computational investigations by Surawatanawong et al. agreed with the results of the previous studies. A high-spin sextet ground state was again computed for the Fe(III)–OOH, and it was reiterated that the weaker Fe–O bond specific to higher-spin states would favor the loss of H_2O_2. Furthermore, the effects of solvation on the active site of SORs were modeled and it was found that the addition of water molecules, which acted as hydrogen-bond donors, stabilized the high-spin state of Fe(III)–H_2O_2 and thus favored the release of H_2O_2 over O–O cleavage [26].

Recent results of calculations using hybrid DFT approaches as well as QM/MM by Sit et al. are in line with those obtained by Solomon and others when describing the protonation sequence and spin states of the putative peroxo intermediate(s). The authors suggested, based on observed spin population and O–O bond lengths, that the reduction of the superoxide moiety to peroxide upon binding to the active site is not spontaneous but rather induced by proton transfer at a later stage of the enzymatic cycle. A role of the residue Lys48 as a proton source in the first protonation step, in line with some previous experimental observations, was additionally confirmed. Moreover, the study showed a hydrogen-bond network between the interstitial water molecules and the imidazole rings of the His ligands in the active site that would modulate superoxide binding to iron [27].

Niviere and co-workers [11] reported experimental data indicating that, under special conditions, O–O bond cleavage with the formation of a high-valent iron state at the active site of SORs can be observed. These special conditions involve a large excess of peroxide, and, most importantly, the use of a mutation in which Lys48 is replaced with a hydrophobic residue [11]. The interpretation was that, during the SOR catalytic cycle, protonation of the ferric hydroperoxo intermediate needs to be conducted at the iron-bound oxygen atom in efficient manner in order to avoid other reaction pathways, and Lys48 is essential in this protonation. While the proton affinities of the two oxygen atoms within an SOR ferric hydroperoxo species were predicted to be significantly different from each other and to favor protonation of the iron-bound oxygen atom [20], it may be expected that, in the absence of a specific catalyst, the steric limitations imposed by the histidine ligands around the iron [20] may in fact limit this protonation, hence allowing the undesirable protonation at the OH oxygen atom of the ferric hydroperoxo species, leading to accidental oxygen–oxygen bond cleavage.

On a different note, Niviere and co-workers also found that an unprotonated ferrous superoxo state is also observable prior to the ferric hydroperoxo species. Hoffman and co-workers [28] have shown that, even at temperatures as low as 4 K, such ferrous superoxo/ferric peroxo species may undergo protonation to yield a ferric hydroperoxo state. The stability of the $[FeOO]^+$ moiety with respect to protonation in *non*-heme enzymes is still likely to offer interesting findings from an experimental point of view [29]. On the computational side, our DFT methodology cannot as yet provide predictions where the SOR ferrous superoxo state (unprotonated at either of the oxygen atoms) constitutes a local minimum in the presence of a proton source such as Lys48; this is in line with experimental observations of model systems, where such ferrous superoxo states require low temperatures and aprotic solvents [29].

The study described in the present paper was an investigation of the relative preferences for Fe–O versus O–O bond cleavage in SOR reaction intermediates. We examined not only the ferric hydroperoxo adducts that are generally thought to be key to the catalytic cycle, but also their protonated versions, Fe(III)–H_2O_2, as these are feasible SOR intermediates as well. Moreover, unlike in previous studies, we also examined ferrous hydroperoxo and ferrous H_2O_2 adducts, given that the "as-isolated" forms of some SORs are ferrous, and a number of studies have attempted to generate and study possible SOR reaction intermediates via the reaction of such a ferrous form with

hydrogen peroxide [9, 11]. In contrast to previous computational studies, we found that O–O bond cleavage in SOR is not entirely impossible, even though it is greatly disfavored; nevertheless, this O–O bond cleavage was computed to be feasible in ferrous hydrogen peroxide species, but not in the ferric ones known to be important in the SOR catalytic cycle.

Materials and methods

Among the available structures of SORs, the one-iron active center of the B chain of the PDB SOR structure (1DQI) was selected for computational investigation. For most of the models reported here, the axial cysteinate was modeled as a methyl thiolate and the equatorial histidines were modeled as ammonia. Calculations were also performed where the histidines were modeled as imidazoles; these results were qualitatively similar to those obtained for the smaller models, and are therefore presented only in the Electronic supplementary information (ESM); indeed, despite our initial claims that the exact orientation of the imidazole rings influences the binding of superoxide to the iron, none of the studies performed subsequently have confirmed this hypothesis [20]; indeed, studies such as [23] proved that simply modeling the histidines as ammonia can provide meaningful results. Hydroperoxo or hydrogen peroxide axial ligands were placed *trans* to the thiolate in the ferrous and ferric forms, with the overall charge adjusted accordingly (considering the monoanionic character of the hydroperoxide and thiolate and the electrically neutral character of the hydrogen peroxide and histidine/ammonia). Computed geometric parameters, Mulliken atomic spin densities, Mulliken atomic charges, and relative energies for all models are summarized in the ESM.

Energy profiles for both Fe–O and O–O bond cleavage were investigated using the coordinate driving function within Gaussian 09 [30], with GaussView [31] employed as the front end. Optimizations were carried out using the hybrid meta GGA (M06-2X) DFT method [32] and the 6-31G(d,p) basis set on an IBM HPC cluster.

Solvation calculations were performed for all complexes. Starting from geometries that had already optimized in vacuum, the energy was determined by single-point calculations employing the CPCM solvation model [33] implemented in Gaussian 09. Water was used as solvent (as the SOR site is indeed solvent-exposed [7]) and the triple zeta 6-311 + G(d,p) was used as the basis set. Energy profiles were generally computed up to the full extent of the van der Waals radius for Fe–O and O–O (3.52 and 3.04 Å, respectively). These data, with larger basis sets and with solvation, did not affect the trends discussed in the main text, and are listed in the ESM.

Results and discussion

As illustrated in Figs. 2 and 3, the M06-2X functional predicts $S = 5/2$ to be the ground state in the putative ferric peroxo and ferric hydrogen peroxide SOR reaction intermediates, by ~10–30 kcal/mol. The geometric parameters for the equilibrium structures as well as the spin densities and partial atomic charges, which are listed in the ESM, are in agreement with previously reported data for similar models. As previously discussed, the high-spin states unavoidably lead to longer iron–ligand bonds, thus including a weakening of the Fe–O bond preferentially over O–O and favoring hydrogen peroxide release over oxygen–oxygen bond cleavage [23, 25, 34–38]. Further-

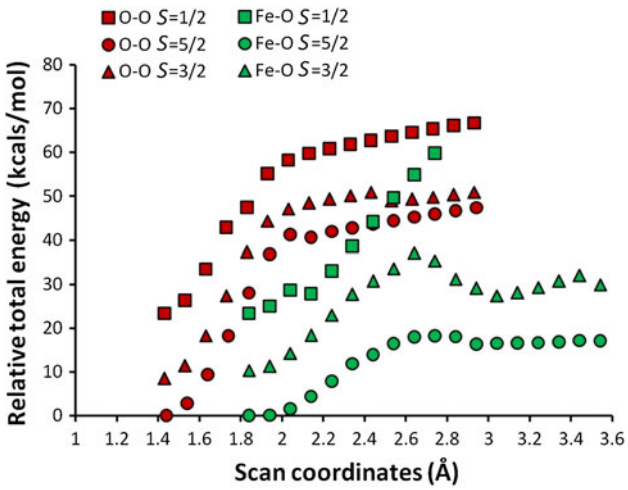

Fig. 2 Energy profiles of Fe–O and O–O for a putative ferric hydroperoxo SOR reaction intermediate; the equilibrium energy of the high-spin state was taken as an arbitrary reference

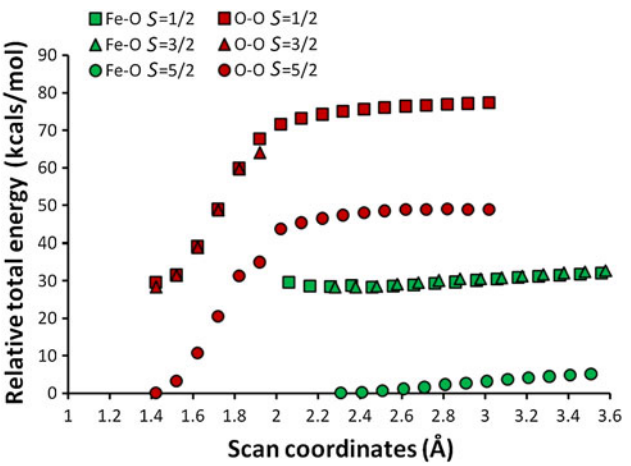

Fig. 3 Energy profiles of Fe–O and O–O for a putative ferric hydrogen peroxide SOR reaction intermediate; the equilibrium energy of the high-spin state was taken as an arbitrary reference

more, for the H_2O_2 adducts, the Fe–O bond is significantly elongated compared to that for the hydroperoxo adducts; in the high-spin states, the differences are 0.3–04 Å for both the ferrous and the ferric models, suggesting that this second protonation would additionally favor Fe–O bond cleavage.

The energy profiles in Figs. 2 and 3 illustrate that the energy cost of O–O cleavage in both the ferric hydroperoxo and ferric hydrogen peroxide exceeds 47 kcal/mol, 30 kcal higher than the energy required to elongate the Fe–O bond in Fe(III)–OOH. Moreover, the energy cost of elongating the Fe–O bond in Fe(III)–H_2O_2 is essentially zero. Thus, Fe–O bond cleavage is greatly favored over O–O bond cleavage in SOR ferric peroxo adducts. Importantly, besides the high energies required for O–O bond cleavage, we were not able to locate a local minimum corresponding to a structure featuring a broken O–O bond when starting from a ferric hydroperoxo structure, regardless of spin state, thus suggesting that such a process is disfavored on thermodynamic as well as kinetic grounds.

Similarly to what was seen in the ferric cases, Figs. 4 and 5 show that the high-spin state ($S = 2$) is computed to be the ground state in Fe(II)–OOH^- as well as in Fe(II)–H_2O_2. The energy profiles for Fe–O bond elongation show energy costs of approximately 13 kcal/mol for Fe(II)–OOH^- and essentially zero for Fe(II)–H_2O_2. The extremely low barriers to Fe–O bond cleavage in ferrous as well as ferric H_2O_2 models suggest that, unlike the hydroperoxo species, hydrogen peroxide adducts are very unlikely to be observed experimentally in SOR. Nevertheless, they could be proposed as formal intermediates, especially in SOR mutants lacking the distal E47 residue; at least, based on the data from Figs. 2 and 3, the dissociation of H_2O_2 from

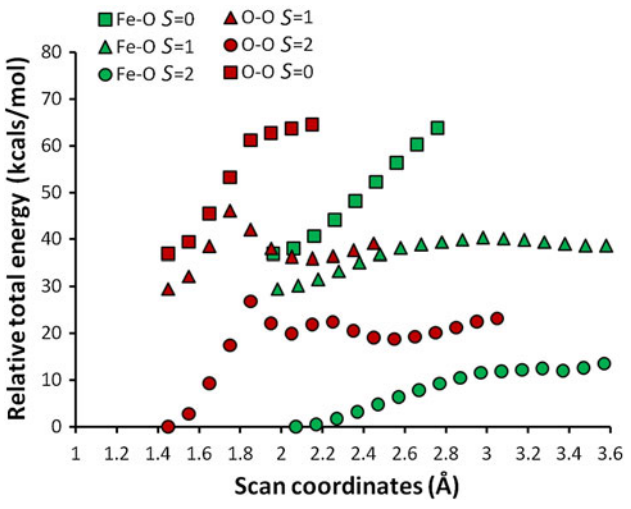

Fig. 4 Energy profiles of Fe–O and O–O for the ferrous hydroperoxo complex; the equilibrium energy of the high-spin state was taken as an arbitrary reference

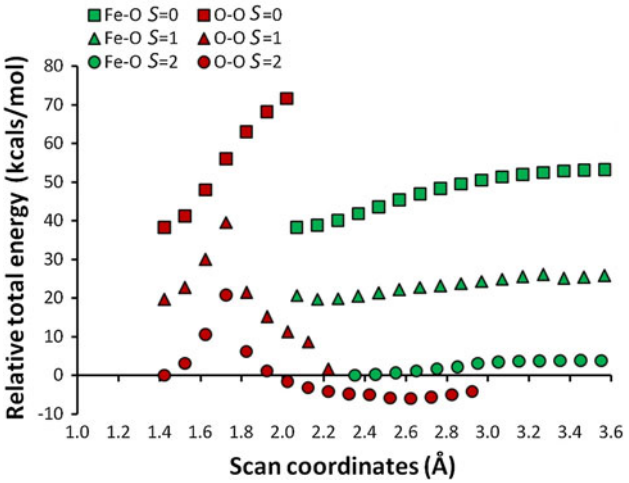

Fig. 5 Energy profiles of Fe–O and O–O for the ferrous hydrogen peroxide complex; the equilibrium energy of the high-spin state was taken as arbitrary reference

ferric or ferrous SOR is much simpler/faster than the dissociation of HOO^-.

For O–O cleavage, low-spin ferrous states require energies of at least ~30 kcal/mol, although—as was the case for the ferric models of Figs. 2 and 3—a local minimum corresponding to a product was not located, even at 30 kcal/mol. Remarkably, unlike in the ferric case, a reasonably small barrier (~15 and ~25 kcal/mol, respectively) was identified for O–O bond cleavage in two of the ferrous hydroperoxo spin states—the $S = 1$ and the ground-state $S = 2$. Similarly small barriers were computed (cf. Fig. 5) for the ferrous hydrogen peroxide models. Even though these barriers to O–O bond cleavage in ferrous hydroperoxo/hydrogen peroxide models appear to be higher than those leading to Fe–O bond cleavage, this suggests that O–O bond cleavage may in fact be detectable in SORs as a very minor side reaction under particular conditions (e.g., in the presence of large amounts of substrate, when even minor side reactions may be detected, and/or certain factors affecting the spin state, such as temperature and possible "allosteric" binding of non-substrates near the active site), and that this event would be more likely to happen with ferrous SORs than with ferric SORs. This is consistent with recent findings revealing that O–O bond cleavage in ferrous peroxo model compounds is facile [39]. The relative feasibility of O–O bond cleavage within a hydrogen peroxide adduct in the absence of a catalyst is in accord with previous findings on heme and non-heme systems [40].

We have previously commented on how ferrous iron is indeed more adept than ferric iron at activating a peroxo ligand; electron-rich ligands (such as thiolate) would work along the same lines [24, 41]. Thus, when comparing octahedral ferric hydroperoxo models where the remaining

five ligands are water and hydroxide in ratios varying from 5:0 to 0:5, the O–O bond lengths and population analyses clearly revealed a tendency of the anionic ligands to favor O–O bond cleavage—so much so that, in certain models, the bond was broken simply upon performing geometry optimization [24]. Thiolate was shown to have a very similar effect to other anionic ligands [22, 24]. In heme systems, a similar trend towards slight weakening of the O–O bonds was noted when comparing ferrous hydroperoxo with ferric hydroperoxo systems [41].

In addition, energy profiles for Fe–O and O–O were computed in water for all models. Graphical presentations of the solvated energy profiles can be found in the ESM. All profiles followed the same pattern as the profiles computed in vacuum, with only minor differences (in the form of lower differences in relative energies). Also, as a side issue, two of the energy profiles in Figs. 2 and 4 appear to have more than one maximum. This is due to the involvement of the hydroxide/hydroperoxide moiety in hydrogen bonding with the neighboring equatorial ligands during the scanning process. Such events were only detectable in a few scanning steps and entail only small energy changes, with no apparent effect on the qualitative conclusions of this report.

Examination of the electronic structures of the models on the right sides of the plots in Figs. 2, 3, and 4, at the longest Fe–O or O–O bond distances, may provide insight into the homolytic versus heterolytic nature of the respective bond-cleavage processes; detailed numerical data for all spin states and models are given in the ESM. For the ferric hydroperoxo models, cleavage of the Fe–OOH bond leads to an OOH moiety with an O–OH bond of 1.43 Å, a charge of −0.35, and negligible spin density, consistent with dominant hydroperoxide character; likewise, the iron in the $S = 5/2$ state harbors more than four spin units, consistent with ferric character. This finding also implies that an incoming protonated superoxide, OOH^0, would in fact be reduced by the ferrous SOR iron in an essentially outer-sphere process, and gain significant hydroperoxide character well before a proper Fe–OOH bond could be established. Solvation calculations performed in water further enhance this tendency. We have previously drawn similar conclusions about certain steps associated with superoxide dismutase enzymes [42]. By contrast, as discussed in the "Introduction," there appears to be a general consensus against outer-sphere (and even inner-sphere) electron transfer between ferrous SORs and unprotonated superoxide, OO^-; as the pK_a of free superoxide is ~4.8, substrate molecules would be expected to approach the SOR active site mainly in their unprotonated forms. On the other hand, the data in the ESM show that there are no unexpected data regarding Fe–O bond cleavage in the ferric and ferrous H_2O_2 models—clean liberation of hydrogen peroxide is observed.

Cleavage of the O–OH bond in the ferric Fe–OOH models, regardless of the spin state, produces one unpaired electron and essentially zero charge on the departing OH moiety—in other words, homolytic cleavage leading to a hydroxyl radical and a formally Fe(IV) center. By contrast, the ferrous models lead to essentially zero spin and negative charge on the departing OH—indicative of heterolytic cleavage. On the other hand, in the Fe–H_2O_2 models, not only the ferric models but also the ground-state $S = 2$ Fe(II)–H_2O_2 model feature homolytic cleavage. Energy calculations of a hypothetical heterolytic pathway for both $S = 5/2$ Fe(III)–H_2O_2 and Fe(II)–H_2O_2 confirm that the homolytic pathway is favored (see the ESM); however, these numbers offer only a qualitative estimate, as they do not account for a possible donor of a second proton to the departing hydroxide/hydroxyl moiety.

The present study identifies the ferrous peroxo pathway as a potential source of O–O bond cleavage in SORs; while this pathway has limited feasibility, it is not impossible. It remains to be seen whether other routes to high-valent iron in SORs are also possible. These findings correlate well with those of Niviere and co-workers on O–O bond cleavage in SORs: indeed, in their experiments showing the formation of high-valent iron, the reagents were hydrogen peroxide and a *ferrous* SOR. The fact that O–O bond cleavage was reported in K48I but not in wild-type SORs can at first sight only be interpreted as proof that K48 is key to selectively protonating the iron-bound oxygen atom in a ferric (or even in a ferrous) hydroperoxo adduct. This conclusion is nevertheless disconcerting in the context where K48 is free to move in a relatively unrestricted manner above the iron in SORs; except for K48 and E47, which are free to come to within 3 and 2 Å of the iron, respectively [7], the sixth coordination position at the iron (*trans* to the cysteinate) remains completely solvent-exposed. From this point of view, in a context where it has reasonable conformational freedom, K48 could in principle approach any of the two oxygen atoms in SORs, not necessarily only the iron-bound one; after all, as shown by Figs. 2, 3, 4, and 5, even in the absence of a catalyst, Fe–O bond cleavage is still extremely favored over O–O bond cleavage. If so, then the result of the K48I mutation should be interpreted as a modification of the distal environment in a way that limits the accessibility of protons to the iron-bound oxygen atom, perhaps by the Ile side-chain itself; this steric limitation would then allow more chances for the second protonation event to occur at the non-iron-bound oxygen atom of a ferric hydroperoxo species.

To conclude, this work represents the first reported comparison of the energy profiles for O–O and Fe–O bond cleavage in ferric versus ferrous adducts of SORs with hydroperoxide and hydrogen peroxide. These data enable a

more informed estimation of the probability of observing a high-valent state in SORs.

Acknowledgments Funding from the Romanian Ministry for Education and Research (grant PCCE ID 140/2008) is gratefully acknowledged. Drs. DM Kurtz, Jr. (UTSA), Z.A. Kun, and M.-M. Uta (BBU) are thanked for helpful discussions.

References

1. Abreu IA, Saraiva LM, Carita J, Huber H, Stetter KO, Cabelli DE, Teixeira M (2000) Mol Microb 38:322–334
2. Jenney FE, Verhagen MF, Cui XY, Adams WW (1999) Science 286:306–309
3. Lombard M, Fontecave M, Touati D, Nivière V (2000) J Biol Chem 275:115–121
4. Jovanovic T, Ascenso C, Hazlett KRO, Sikkink R, Krebs C, Litwiller R, Benson LM, Moura I, Moura JJG, Radolf JD, Huynh B, Naylor S, Rusnak F (2000) J Biol Chem 275:28439–28448
5. Coulter ED, Emerson JP, Kurtz DM Jr, Cabelli DE (2000) J Am Chem Soc 122:11555–11556
6. Rodrigues JV, Saraiva LM, Abreu IA, Teixeira M, Cabelli DE (2007) J Biol Inorg Chem 12:248–256
7. Yeh A, Hu Y, Jenney FJ, Adams M, Rees D (2000) Biochemistry 39:2499–2508
8. Coelho A, Matias P, Fulop V, Thompson A, Gonzalez A, Carrondo M (1997) J Biol Inorg Chem 2:680–689
9. Kurtz DM Jr (2004) Acc Chem Res 37:902–908
10. Rodrigues JV, Abreu IA, Cabelli D, Teixeira M (2006) Biochemistry 45:9266–9278
11. Bonnot F, Molle T, Ménage S, Moreau Y, Duval S, Favaudon V, Houée-Levin C, Niviere V (2012) J Am Chem Soc 134: 5120–5130
12. Emerson JP, Coulter ED, Cabelli DE, Phillips R, Kurtz DM Jr (2002) Biochemistry 41:4348–4357
13. Huang VW, Emerson JP, Kurtz DM Jr (2007) Biochemistry 46:11342–11351
14. Mathé C, Mattioli TA, Horner O, Lombard M, Latour JM, Fontecave M, Nivière V (2002) J Am Chem Soc 124:4966–4967
15. Mathé C, Nivière V, Houée-Levin C, Mattioli TA (2006) Biophys Chem 119:38–48
16. Horner O, Mouesca JM, Oddou JL, Jeandey C, Nivière V, Mattioli TA, Mathé C, Fontecave M, Maldivi P, Bonville P, Halfen JA, Latour JM (2004) Biochemistry 43:8815–8825
17. Testa F, Mastronicola D, Cabelli DE, Bordi E, Pucillo LP, Sarti P, Saraiva LM, Giuffrè A, Teixeira M (2011) Free Radic Biol Med 51:1567–1574
18. Bonnot F, Houée-Levin C, Favaudon V, Nivière V (2010) Biochim Biophys Acta 1804:762–767
19. Katona G, Carpentier P, Niviere V, Amara P, Adam V, Ohana J, Tsanov N, Bourgeois D (2007) Science 316:449–453
20. Silaghi-Dumitrescu R, Silaghi-Dumitrescu I, Coulter ED, Kurtz DM Jr (2003) Inorg Chem 42:446–456
21. Clay MD, Emerson JP, Coulter ED, Kurtz DM Jr, Johnson MK (2003) J Biol Inorg Chem 8:671–682
22. Silaghi-Dumitrescu R (2008) Rev Roum Chim 53(12):1149–1156
23. Dey A, Solomon E (2010) Inorg Chim Acta 363:2762–2767
24. Silaghi-Dumitrescu R (2004) Proc Rom Acad Series B 3:155–163
25. Dey A, Jenney F Jr, Adams MW, Johnson MK, Hedman B, Hodgson KO, Solomon EI (2007) J Am Chem Soc 129:12418–12431
26. Surawatanawong P, Tye JW, Hall MB (2010) Inorg Chem 49:188–198
27. Sit PH-L, Migliore A, Ho M-H, Klein M-L (2010) J Chem Theory Comput 6:2896–2909
28. Hoffman BM (2003) Acc Chem Res 36:522–529
29. McDonald AR, Van Heuvelen KM, Guo Y, Li F, Bominaar EL, Münck E, Que L Jr (2012) Angew Chem Int Ed 51:9132–9136
30. Frisch MJ, Trucks GW, Schlegel HB, Scuseria GE, Robb MA, Cheeseman JR, Scalmani G, Barone V, Mennucci B, Petersson GA, Nakatsuji H, Caricato M, Li X, Hratchian HP, Izmaylov AF, Bloino J, Zheng G, Sonnenberg JL, Hada M, Ehara M, Toyota K, Fukuda R, Hasegawa J, Ishida M, Nakajima T, Honda Y, Kitao O, Nakai H, Vreven T, Montgomery JA Jr, Peralta JE, Ogliaro F, Bearpark M, Heyd JJ, Brothers E, Kudin KN, Staroverov VN, Kobayashi R, Normand J, Raghavachari K, Rendell A, Burant JC, Iyengar SS, Tomasi J, Cossi M, Rega N, Millam NJ, Klene M, Knox JE, Cross JB, Bakken V, Adamo C, Jaramillo J, Gomperts R, Stratmann RE, Yazyev O, Austin AJ, Cammi R, Pomelli C, Ochterski JW, Martin RL, Morokuma K, Zakrzewski VG, Voth GA, Salvador P, Dannenberg JJ, Dapprich S, Daniels AD, Farkas Ö, Foresman JB, Ortiz JV, Cioslowski J, Fox DJ (2009) Gaussian 09, revision A.1. Gaussian, Inc., Wallingford
31. Dennington R II, Keith T, Millam J, Eppinnett K, Hovell WL, Gilliland R (2003) GaussView, version 3.09. Semichem, Inc., Shawnee Mission
32. Zhao Y, Truhlar DG (2008) Theor Chem Acc 120:215–241
33. Cossi M, Rega N, Scalmani G, Barone V (2003) J Comp Chem 24:669–681
34. Kovacs JA (2004) Chem Rev 104:825–848
35. Solomon EI (2003) Proc Natl Acad Sci USA 100:3589–3594
36. Lehnert N, Ho RYN, Que LJ, Solomon EI (2001) J Am Chem Soc 122:12802–12816
37. Lehnert N, Ho RYN, Que LJ, Solomon EI (2001) J Am Chem Soc 123:8271–8290
38. Solomon EI (1996) Chem Rev 96:2239–2314
39. Li F, England J, Que L Jr (2010) J Am Chem Soc 132:2134–2135
40. Silaghi-Dumitrescu R (2007) Studia Univ Babes-Bolyai Ser Chem 52:47–54
41. Silaghi-Dumitrescu R (2004) Arch Biochem Biophys 424:137–140
42. Silaghi-Dumitrescu R (2009) J Mol Graph Model 28:156–161